

Coda-Wave Monitoring of Continuously Evolving Material Properties and the Precursory Detection of Yielding

Reuben Zotz-Wilson, Thijs Boerrigter, Auke Barnhoorn

Abstract—The nominally incoherent coda of a scattered wavefield has been shown to be a remarkably sensitive quantitative monitoring tool. Its success is however often underpinned by the assumption of a moderate velocity perturbation, and in the absence of notable changes in material scattering properties. The deformation of a rock matrix, represents for a monitoring wavefield pronounced changes in scattering power. In this work we introduce a rolling reference wavefield when applying Coda-Wave Interferometry (CWI) and Coda-Wave-Decorrelation (CWD) in order to monitor relative velocity and material scattering power changes. We demonstrate how this modification enables the qualitative monitoring of stages in material deformation common to Unconfined Compressive Strength (UCS) tests. In addition to the general stages of deformation, the precursory/subtle onset of material yielding is identifiable in both the CWI and CWD method. It is therefore expected that this approach will enable these coda based methods to robustly monitor continuous, destructive processes over a variety of scales. Possible applications include fault, induced seismicity, landslide and critical infrastructure monitoring.

I. INTRODUCTION

With the advent of affordable sensor networks, along with the ability to transmit large amounts of data wirelessly, the feasibility of evermore complex monitoring systems is increasing rapidly (Brownjohn, 2007; Staehli et al., 2015). Whether it be critical infrastructure structural health monitoring (bridges, dams, nuclear reactors) or environmental hazards (earthquakes, landslides, induced seismicity) early warning detection to dynamic failure, continuous non-intrusive monitoring is crucial. Many works have demonstrated the remarkable sensitivity of the scattered coda wave to media-wide properties, through the estimation of velocity changes over fault zones (Poupinet et al., 1984), in volcanoes (Ratdomopurbo and Poupinet, 1995; Matsumoto et al., 2001; Grêt, 2005; Sens-Schönfelder and Wegler, 2006), and within the lunar near surface (Sens-Schönfelder and Larose, 2008). Various ultrasonic laboratory experiments have shown the coda's sensitivity to changes at the mesoscopic scale in terms of stress, temperature, and water saturation (Stähler et al., 2011; Zhang et al., 2012; Grêt et al., 2006). The Coda-Wave Interferometry (CWI) formulation presented by Snieder et al. (2002) has served as the basis for many such relative time-lapse monitoring studies on solid media. In the field of optics an equivalent formulation to CWI, termed Diffusing Wave Spectroscopy (DWS) (Pine et al., 1990), later extended to acoustics as Diffusing Acoustic Wave Spectroscopy (DAWS) (Page et al., 2000) has shown the

ability to monitor the average displacement of scatterers in a fluidised suspension. In general the recent research applying CWI have focused on exploiting the sensitivity benefits of the coda-wave in monitoring subtle, often cyclical, non-destructive processes and thereby inferring the average velocity change. A related method termed Coda-Wave Decorrelation (CWD) as formalised by Rossetto et al. (2011) provides a spatiotemporal theoretical expression for the resulting decorrelation between a reference and perturbed wavefield due to the addition of a single scatterer. The ability of CWD to locate such a local change in scattering properties with the aid of a maximum likelihood inversion between the measured and theoretical decorrelation has been shown in a laboratory setting (Larose et al., 2010), around an active volcano (Obermann et al., 2013) and most recently on a life-sized reinforced concrete structure (Zhang et al., 2016). The focus of this branch of coda-wave studies is on relating the decorrelation effects of changes in material scattering properties, in contrast to CWI focusing on the phase shift. While this most recent structural health monitoring application of CWD does demonstrate its practical application to identifying the transition from an elastic to inelastic deformation, to the authors' knowledge there has been no published work which applies either CWI or CWD throughout the elastic and inelastic deformation of a material up until dynamic failure. In this study we therefore explore the practical application of coda-wave focused monitoring methods of materials undergoing continuous changes in bulk scattering power and intrinsic velocity, with the goal of identifying the defined stages of material deformation and precursory indicators to material yielding. In particular, we show that for a fixed reference wavefield $u_r(t)$ after only the initial elastic deformation of a material, both CWI and CWD monitoring no longer provide sufficient sensitivity to identify the transition from elastic to inelastic deformation. As an alternative a rolling reference wavefield $u_p(t)$ is employed in the cross-correlation formulation. With this simple modification, we show how one is able to identify three defined phases of material deformation common to laboratory Unconfined Compressive Strength (UCS) tests. From this segmentation we are able to determine for two lithologies and three samples, precursory indicators to a materials yield point in both the CWI and CWD trends.

II. FIXED-REFERENCE MONITORING OF DESTRUCTIVE PROCESSES

A. The Theory of CWI for Monitoring Changes in Velocity

The formulation of CWI as presented by Snieder et al. (2002) rests upon the understanding that a recorded wavefield $u_u(t)$ which has interacted with an unperturbed scattering medium can be represented as the summation of all possible paths P through that medium.

$$u_u(t) = \sum_P A_P(t - t_P), \quad (1)$$

where the amplitude and travel time at the receiver for each path is given by A_P and t_P respectively, which implies that the shape of the wave does not change long the path P . The first major assumption concerning the medium itself is that each individual scatterer has stationary properties, therefore preventing a change in its intrinsic properties such the scattering cross-section (size, shape, density and velocity). Additionally, it is assumed that the mean free path l , which is indirectly related to the averaged distance between scatterers is much greater than the dominant wavelength λ .

A perturbed wavefield $u_p(t)$ which has experienced a subtle change $\delta \ll l$ in either the location of scatterers, the location of the source or the background medium velocity, can then be represented as,

$$u_p(t) = \sum_P A_P(t - \tau_P), \quad (2)$$

where τ_P represents the travel time change along path P . The travel time change itself for each path is defined as $\tau_P = t_P - t_{pP}$, where t_{pP} is the total travel time along path P in the perturbed medium. This formulation therefore implies that no dispersive change is introduced thereby resulting in a phase dominated change in the transmitted wavefield. The Cross-correlation Coefficient $CC(t_s)$ for a particular window within the coda, $(t_k - t_w)$ to $(t_k + t_w)$ is often presented as,

$$CC(t_s) = \frac{\int_{t_k - t_w}^{t_k + t_w} u_u(t) u_p(t + t_s) dt}{\left[\int_{t_k - t_w}^{t_k + t_w} u_u^2(t) dt \int_{t_k - t_w}^{t_k + t_w} u_p^2(t) dt \right]^{1/2}}, \quad (3)$$

where $u_u(t)$ and $u_p(t)$ are the unperturbed and perturbed waveforms respectively. By substituting equations (1) and (2) into equation (3), along with further assumptions on the associated perturbation type and magnitude explained in depth by Snieder (2006) yields,

$$CC(t_s) = 1 - \frac{1}{2} \bar{\omega}^2 \langle (\tau - t_s)^2 \rangle, \quad (4)$$

where $\bar{\omega}$ is the mean-squared angular frequency for the arrivals within $\langle \dots \rangle_{t_k, t_w}$. The $CC(t_s)$ will reach a maximum when the average travel time perturbation $\langle \tau \rangle = t_s$, at which point $\langle (\tau - t_s)^2 \rangle$ is equal to the variance σ_τ^2 of the travel time perturbations τ . This essentially relates CC_{max} value with the variance $\langle (\tau - t_s)^2 \rangle$ of the travel time perturbation from the recorded data by,

$$CC_{max} = 1 - \frac{1}{2} \bar{\omega}^2 \sigma_\tau^2. \quad (5)$$

A homogeneous relative velocity perturbation can then be determined to a first order approximation by,

$$\frac{\delta v}{v} = - \frac{\langle \tau \rangle}{t} \quad (6)$$

If we now consider this in terms of a rock matrix the first assumption of CWI implies that the size, width and number of inhomogeneities (e.g. fractures, pores) remains constant in time. Furthermore, it requires that the average distance between such inhomogeneities is much greater than the dominant wavelength λ . The constraint of a non-dispersive perturbation requires that changes in properties such as scattering or intrinsic attenuation are negligible. Provided only a subtle, cyclical, elastic deformation is applied to a medium, these assumptions generally hold within the time period between the perturbed and unperturbed wavefield. This is demonstrated in the work by Grêt et al. (2006) where velocity changes are observed for a sandstone core sample due to a subtle elastic increase in uniaxial stress.

B. Applying a CWD Approach to Monitoring Changes in Scattering Properties

In order to enable the coda based monitoring of scenarios where inelastic material deformation occurs one can focus on the CC_{max} relationship with a materials total scattering cross-section σ_T , instead of the $t_s = \langle \tau \rangle$ at which its maximum is found. This is equivalent to the Coda-Wave Decorrelation methods discussed earlier, though with the distinction that here the main goal is not to find a localised scatterer perturbation within the medium but to monitor a global perturbation within the region sampled by the coda-wave.

The two phenomenological parameters which control the shape and amplitude of coda waves are the total scattering coefficient g_0 and the coda-wave attenuation Q_c^{-1} Aki and Chouet (1975). Here a scattering media is modelled as a random distribution of point-like scatterers with number density ρ_n , within a background velocity V_0 . For a propagating plane wave the medium total scattering coefficient is given by,

$$g_0 = \frac{1}{4\pi} \oint g d\Omega = \rho_n \oint \frac{d\sigma}{d\Omega} d\Omega = \rho_n \sigma_T \equiv l^{-1}. \quad (7)$$

The ratio $d\sigma/d\Omega$ is the differential scattering cross-section per solid angle $d\Omega$, and can be thought of as a normalised measure of the energy scattered into $d\Omega$ per unit time, dependent on the incident wave frequency content and the scatterer size. The scattering power per unit volume is defined by $g = 4\pi \rho_n d\sigma/d\Omega$. For an angular frequency ω and background velocity V_0 , the attenuation due to scattering is related to g_0 as Sato et al. (2012),

$$s_c Q^{-1}(\omega) = \frac{g_0 V_0}{\omega}. \quad (8)$$

Considering these two parameters in terms of the evolution of a materials scattering properties, the increase or decrease in size or impedance contrast of scatterers will increase or decrease g_0 and Q_c^{-1} as the total energy scattered into $d\Omega$ changes. The addition or removal of scatterers from the medium will

have a similar affect, as the number density ρ_n changes. In terms of equation (3) this will result in a decorrelation ($K(t_s) = 1 - CC(t_s)$) between the unperturbed and perturbed states. The work by Rossetto et al. (2011) formalised this understanding by applying diffusive propagation theory to derive an expression for the theoretical decorrelation coefficient $K(\mathbf{X}_p, t)$ which would result due to the perturbation of a single scatterer at location \mathbf{X}_p within a background scattering medium. Re-writing this expression explicitly in terms of unperturbed and perturbed medium states gives,

$$K(\mathbf{X}_p, t, t_{p-u}) = \frac{V_0}{2} \left| \frac{d\sigma_T}{dt_{p-u}} \right| Q(\mathbf{s}, \mathbf{X}_p, \mathbf{r}, t), \quad (9)$$

where $Q(\mathbf{s}, \mathbf{X}_p, \mathbf{r}, t)$ is the sensitivity kernel of the medium with a source \mathbf{s} and receiver \mathbf{r} for a time t within the coda. The change in σ_T at location \mathbf{X}_p between the unperturbed and perturbed states is defined by $|d\sigma_T/dt_{p-u}|$. We will define the volume of the sensitivity kernel is as $V_{Q(\mathbf{s}, \mathbf{X}_p, \mathbf{r}, t) > SNR}$, where $Q(\mathbf{s}, \mathbf{X}_p, \mathbf{r}, t)$ is greater than the Signal to Noise Ratio. If one assumes a random, homogeneous and isotropic perturbation of $n = \rho_n V_{Q(\mathbf{s}, \mathbf{X}_p, \mathbf{r}, t) > SNR}$ identical scatterers within this volume at a fixed time t , the subsequent decorrelation can be defined as,

$$K(\mathbf{X}, t_{p-u}) = \frac{V_0}{2} \left| \frac{d\sigma_T}{dt_{p-u}} \right| \int_{i=0}^n Q(\mathbf{s}, \mathbf{X}_i, \mathbf{r}, t) dn, \quad (10)$$

where $Q(\mathbf{s}, \mathbf{X}_i, \mathbf{r}, t)$ is now defined for the ensemble of weak perturbations in $|dg_0/dt_{p-u}|$ at locations $\langle \mathbf{X}_i \rangle$. With equation (7) this can be written in terms of g_0 as,

$$K(\mathbf{X}, t_{p-u}) = \frac{V_0}{2} \left| \frac{dg_0}{dt_{p-u}} \right| \int_{i=0}^n Q(\mathbf{s}, \mathbf{X}_i, \mathbf{r}, t) dV_{Q > SNR}. \quad (11)$$

As equation (11) is only a function of g_0 for the time interval dt_{p-u} , with an increase/decrease in a materials scattering coefficient we can expect the decorrelation coefficient to monotonically increase/decrease respectively. In the limit of either continuous transient or high rate-of-change perturbations $K(\mathbf{X}, t_{p-u})$ will approach unity, after which point the system will no longer provide any information on any further changes. In practice any measured decorrelation coefficient between two recorded time-series is unlikely reach one due to the serially correlated nature of geophysical time-series data (Ebisuzaki, 1997), where the auto-correlation is non-zero for a non-zero lag. At this extreme the coefficient will mealy represent a spurious correlation between two time-series. However, provided that a weak perturbation can be ensured in the interval dt_{p-u} , the measured $K(t_s)$ can be related to the modulus of the change in a materials scattering coefficient weighted by the sensitivity kernel $Q(\mathbf{s}, \mathbf{X}_i, \mathbf{r}, t)$.

III. ROLLING-REFERENCE CODA MONITORING OF DESTRUCTIVE PROCESSES

With the goal of enabling the long term monitoring of continuously evolving material scattering properties, it is proposed to use a rolling reference waveform when determining both the decorrelation coefficient and the relative velocity change. This concept has been applied before, in the CWI

work by Grêt et al. (2006) compared the relative velocity changes over 5°C temperature intervals for a laboratory core sample. However, this was done not to maintain a statistically significant correlation, but with the presentational motivation of making a direct comparison with acoustic emissions in the same intervals. In terms of equation (3) the fixed reference wavefield $u_u(t)$ is replaced by a rolling reference wavefield $u_{p_{j-N}}(t)$, in a monitoring sense lagging behind the most recently acquired wavefield $u_{p_j}(t)$ by N measurements, see equation (12). For convenience in discussion we will hence forth refer to a measured decorrelation coefficient K as,

$$K(t_{p_{j-N}}) = 1 - \frac{\int_{t_k-t_w}^{t_k+t_w} u_{p_{j-N}}(t)u_{p_j}(t+t_s)dt}{\left[\int_{t_k-t_w}^{t_k+t_w} u_{p_{j-N}}^2(t)dt \int_{t_k-t_w}^{t_k+t_w} u_{p_j}^2(t)dt \right]^{1/2}}. \quad (12)$$

Provided the repeat measurement frequency f_m , at which each $u_{p_j}(t)$ wavefield is recorded is sufficient, this formulation provides the flexibility of selecting the reference lag N such that each correlation is able to satisfy the assumptions of CWI and CWD. While a change in the fixed-reference $K(t_{p-u})$ and associated t_s indicates a total change in the scattering power and velocity of the medium in relation to the reference $u_u(t)$, the rolling-reference $K(t_{p_{j-N}})$ represents the change in these properties which occurred between $u_{p_{j-N}}(t)$ and $u_{p_j}(t)$. The equivalent theoretical decorrelation coefficient can be expressed as,

$$K(\mathbf{X}, t_{j-N}) = 1 - \frac{V_0}{2} \left| \frac{dg_0}{dt_{j-N}} \right| \int_{i=0}^n Q(\mathbf{s}, \mathbf{X}_i, \mathbf{r}, t) dV_{Q > SNR} \quad (13)$$

which represents the rate-of-change in g_0 throughout monitoring. We can then relate a relative total change in the decorrelation coefficient K' throughout the monitoring period t_{p-u} to each increment in equation (12) over the same period as,

$$K'(t_s, t_{p-u}) = \int_{t_u}^{t_p} K(t_s, t_{i-1}) dt_{i-1}. \quad (14)$$

With this simple modification we have arrived at an expression which relates the modulus of changes in a materials total scattering coefficient $|dg_0/dt_{p-u}|$ to the decorrelation coefficient, while ensuring the increment between the two compared material states is sufficiently small such that the assumptions of CWI and CWD can be reasonably maintained.

IV. EXPERIMENTAL SETUP

In order to experimentally analyse and compare the attributes of fixed and rolling reference forms of CWI and CWD for continuously evolving scattering properties, acoustic monitoring of an Unconfined Compressive Strength tests on laboratory scale core samples is made, see figure 1. For redundancy, one axially and two radial mounted transducers acting as receivers-RX, and one axially mounted source-TX transducer are attached to the surface of a core sample. Transducers with a peak operating frequency of 1 or 2.25 MHz are used depending on the experiment. In order to reduce the presence of noise, averaging of 512 repeat measurements is made, resulting in a single trace every 15 s. An axially increasing force F is

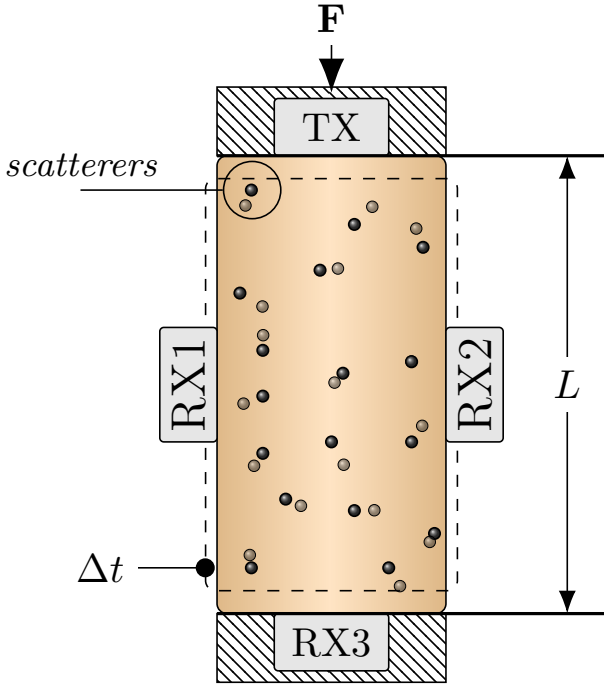


Fig. 1. Schematic representation of the UCS core test setup with active acoustic monitoring. An axially mounted MHz source (TX) with one axial and two radial receives (RX) monitoring the changes in scattering properties every Δt for increasing load F and axial deformation ΔL .

applied to each core sample controlled by a constant axial displacement ($\Delta L/dt$) between $1 - 3 \times 10^{-4} \text{ mm s}^{-1}$. The applied force F and total axial displacement are recorded every half second throughout monitoring up until the sample experiences dynamic failure. The lithologies tested are Bentheimer sandstone (Peksa et al., 2015) which has well sorted grain sizes (180-320 μm and high porosity (21-27 %) and a poorly sorted (30-800 μm , zero primary porosity Granite sourced from Benin. A summary of the three core sample UCS experiments is provided in table I along with the abbreviated sample names employed in this work.

V. CWI AND CWD MONITORING OF AN UCS TEST

Monitoring the evolution of a rock matrix towards dynamic failure with a wavelet at the mesoscopic scale (Li et al., 1998; Heap and Faulkner, 2008; Barnhoorn et al., 2010), is characterised by the continuous evolution of its wavefield propagation properties. For a UCS test this can be illustrated by considering the different stages of material deformation as shown in figure 2 for the BNT1 core sample. Firstly, the initial closure of any existing fractures or pore-space occurs. This is followed by the elastic deformation where a linear stiffening of the rock matrix is expected. These first two stages represent a general reduction in the scattering power of the medium as the size and impedance contrast of the fractures reduce. Finally, the onset of inelastic deformation marks the beginning of fracture growth/formation often termed the Fracture Initiation and Growth Threshold (FIGT). The growth and addition of new fractures represents an irreversible increase in the scattering attenuation $^{Sc}Q^{-1}$ as the materials

scattering power increases. It therefore becomes difficult to apply either CWI or CWD as one cannot assume a phase dominated or weak change in g_0 throughout the UCS tests. Considering first the Coda-Wave Diffusion method, in figure 2 we compare the sensitivity of a fixed K_{fixed} versus a rolling $K_{rolling}$ reference decorrelation coefficient to the stages of material deformation common to UCS tests.

The K_{fixed} coefficient shows a rapid increase over the first 0.025% increase in axial strain, following by a more gradual slope towards 0.7 at the onset of elastic deformation. For the remainder of the USC test K_{fixed} shows little sensitivity to the ongoing deformation, with only a pronounced increase as dynamic failure occurs at 0.56% axial strain. This indicates initial fracture closure represents a large perturbation in g_0 , though after this point K_{fixed} provides little informative value other than the knowledge that some notable change occurred early on during the monitoring period. In comparison, $K_{rolling}$ which is related to the relative rate of change in g_0 as described by equation (13) shows clearly identifiable trends segmenting each of the defined regions of deformation. In order to make a direct comparison with K_{fixed} the scaled (0–1) cumulative integration of $K_{rolling}$ ($K_{rolling}^{int}$) is provided as described by equation (14).

- As with K_{fixed} the initial 0.025% increase in axial strain results in an increase in the rate of change of decorrelation. This indicates an acceleration in dg_0/dt (i.e. the curvature or second derivative $|\ddot{g}_0| > 0$).
- This is followed by a gradual reduction in $K_{rolling}$ where $|\dot{g}_0| > 0$, indicating a reducing rate of fracture closure as the rock matrix stiffens leading up to the beginning of elastic deformation.
- The elastic deformation of the material is characterised by a constant $K_{rolling}$ and therefore \dot{g}_0 , where $|\dot{g}_0| = 0$. Here a unit stiffening of the rock matrix results in a proportional change in g_0 .
- At the FIGT inelastic deformation occurs, which results in an increase in g_0 , where g'_0 and $|\dot{g}_0| > 0$. These changes are reflected by initially a gradual and then steep increase in $K_{rolling}$ all the way until dynamic failure. This is possibly evidence of the sub inelastic region of stable fracture growth before unstable growth continues, noted in literature for crystalline and brittle rocks (Bieniawski, 1967).

Comparing the trend of $K_{rolling}^{int}$ with K_{fixed} a general agreement is evident as both show an initial increase, stabilisation, and then final increase within the region of elastic deformation, however the former clearly shows an improvement in its sensitivity to the underlying perturbations. Most notably, $K_{rolling}^{int}$ reflects the linear nature of the region of elastic deformation and the transition to the non-linear region of elastic fracturing.

In making a similar comparison for Coda-Wave Interferometry monitoring of the BNT1 dataset, the differences in sensitivity between the fixed and rolling reference relative velocity changes are notable, see figure 3. The fixed reference $[\delta v/v]$ shows an initial coherent increase in velocity inline with the Time Of Flight changes $[\delta v/v]^{TOF}$ derived from the

TABLE I
SUMMARY OF THE UCS TESTS CORE SAMPLE LENGTH AND DIAMETER, LITHOLOGY, DISPLACEMENT RATE, AND ACOUSTIC SOURCE FREQUENCY.

	L/D [mm]	Lithology	$\Delta L/dt$ [mm s ⁻¹]	Src. [MHz]
BNT1	75.01/39.75	Bentheimer sandstone	3×10^{-4}	1.0
BNT2	75.11/30.00	Bentheimer sandstone	3×10^{-4}	1.0
GRA	75.70/29.80	Benin granite	1×10^{-4}	2.25

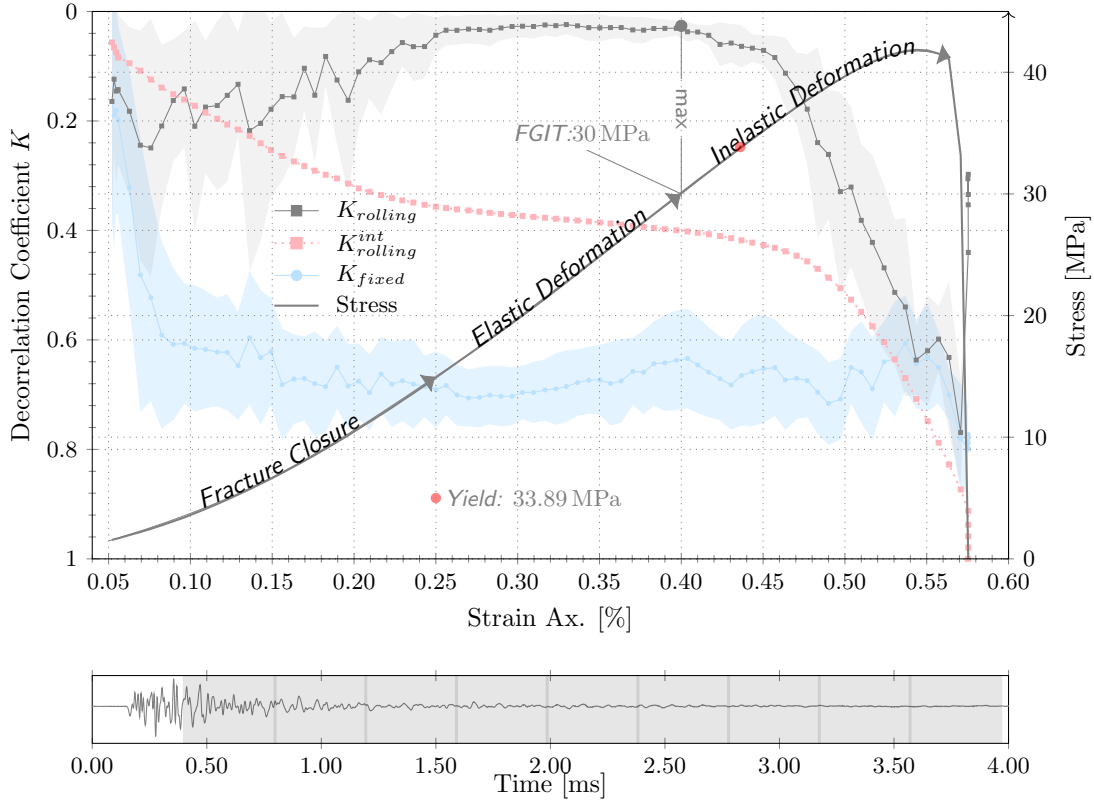


Fig. 2. (color online) CWD monitoring (receiver 2) of BNT1. The mean fixed reference decorrelation coefficient K_{fixed} is compared with the rolling reference equivalent $K_{rolling}$, calculated from 9 independent correlation windows. The $K_{rolling}$ trend is generated with a rolling lag equal to the repeat measurement frequency of 15 s (i.e. $N = 1$). The shaded area represents the standard deviation about the mean decorrelation as calculated from the 0.4 ms correlation windows shown over a single waveform.

first arrivals, though after only the first 0.12% of axial strain its trend appears incoherent. In contrast, the rolling reference cumulative integrated $[\delta v/v]^{int}$ curve tracks the $[\delta v/v]^{TOF}$ curve plateauing over the elastic region. A maximum coda derived relative velocity change occurs at 22.8 MPa whereas the TOF maximum occurs at 35 MPa, indicating the expected sensitivity gain of coda derived methods.

In summary when applying CWD the three stages of material deformation from initial fracture closure, elastic deformation and fracture growth are all reflected in the $K_{rolling}$ and $K_{rolling}^{int}$ trend lines, whereas it is difficult to find any clear segmentation in the K_{fixed} curve. The application of the integrated CWI derived $[\delta v/v]^{int}$, while not able to clearly segment each region of deformation does track the TOF derived changes with improved sensitivity throughout the deformation, whereas the fixed reference $[\delta v/v]$ does not.

VI. PRECURSORY IDENTIFICATION OF MATERIAL YIELDING

Based on the presented ability of both $K_{rolling}$ and $[\delta v/v]^{int}$ to monitor deformation of a rock matrix, we will now assess these methods sensitivity to the onset of inelastic deformation. The yield point of a material is often defined as the transition from predominantly stable fracture growth to predominantly unstable fracture growth (Bieniawski, 1967; Mogi, 2007), while others define it as the point the first micro-fractures are formed (Elliott and Brown, 1986; Paterson and Wong, 2005). There is however, general consensus that the yield point can be identified on a stress/strain diagram as the onset of non-linear behaviour which follows a linear elastic region. This parameter is of critical importance in the prediction of dynamic material failure as it signifies that permanent material deformation has begun. Typically, the yield point from a UCS test would be determined by hand, though in order to remove some of the ambiguity surrounding this, an automated search is made based on the method described in

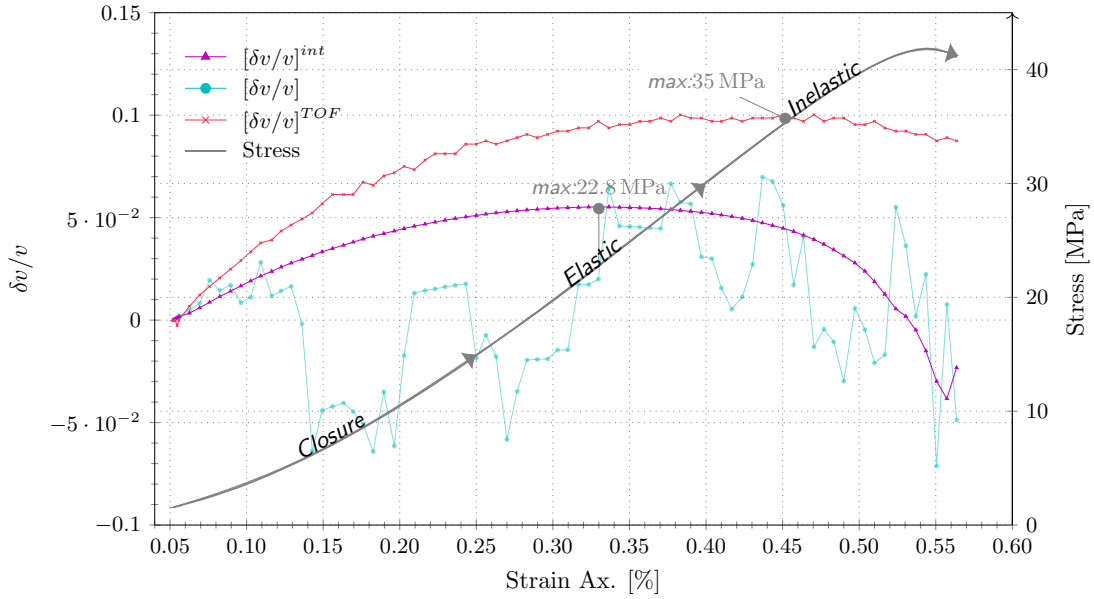


Fig. 3. (color online) CWI monitoring (receiver RX2) of the BNT1 dataset. The mean fixed reference $[\delta v/v]$ relative velocity change is compared with the equivalent cumulative integration of rolling reference $[\delta v/v]^{int}$ for the 9 windows shown in figure 2. For comparison the Time Of Flight derived $[\delta v/v]^{TOF}$ is provided.

the Appendix. On the basis of this search criterion, the yield point can be determined and the precursory/subtle detection capabilities of the CWD and CWI derived methods can be assessed.

For this purpose two additional UCS tests, a repeat Bentheimer (figure 4 - BNT2) and Benin granite (figure 5 - GRA) sample are analysed. As with BNT1, the indication of inelastic deformation (FIGT) is identified at the end of the trough in $K_{rolling}$ as the rate of change in g_0 increases. Similarly, the coda and first arrival derived relative velocity change inelastic indicators are identified at the onset of a reduction in velocity as a result of the acousto-elastic stress effect. In order to make a comparison between the different lithologies and datasets, each precursory indicator is quoted in terms of the percentage of the yield stress at which it is found, as presented in figure 6.

For the Bentheimer sandstone samples (BNT1 and 2) the CWI integrated relative velocity changes $[\delta v/v]^{int}$ indicate the onset of yielding at around 70% of the yield stress, where the CWD decorrelation coefficient $K_{rolling}$ begins to increase at around 86% of the yield stress. The GRA sample on the other-hand show $K_{rolling}$ as providing the earliest indication of inelastic deformation at 66% in comparison to $[\delta v/v]^{int}$ at 89% of yield stress. This may be a result of the differences between the well sorted quartz grains of the Bentheimer sandstone and the poorly sorted crystalline grains of the Benin granite resulting in reduced sensitivity to the acousto-elastic effect. (AUKE: Do you have a reference which explains this point? Basically differences in sensitivity to stress related changes in velocity due to the different sizes of fractures which are formed. I can imagine that a sandstone would fail in a dramatically different way to such a granite.)

In all cases the reference $[\delta v/v]^{TOF}$ show no precursory indicative power to material yielding with the onset of decay occurring after the stress-strain identified yield point. (AUKE:

do you have any reference explicitly states this?, the first arrival velocity changes show no precursory indication to a rock matrix yield point.)

VII. DISCUSSION AND CONCLUSIONS

In this study, we have shown that by applying a rolling reference waveform in both the CWI and CWD form, one is able to monitor the evolution of a materials relative velocity and scattering coefficient where large perturbation is stress occur. Furthermore, we demonstrate that both approaches provide precursory indication of material yielding as defined from stress-strain measurements. While these benefits have direct applications in terms of providing a better understanding of rock properties in the laboratory, it is expected that such a processing approach will enable a wider range of field scale monitoring applications. We suggest that this rolling reference coda monitoring approach is particularly well suited to continuous monitoring applications where early warning detection to material yielding is required. The study by Zhang et al. (2016) which applied fixed reference CWI and CWD to monitoring the inelastic changes in structural concrete is one such application. In that work, the authors noted the increase in error of both the relative velocity and decorrelation coefficient as inelastic deformation progresses, an issue which the present study indicates can be overcome.

An active source landslide monitoring scenario is an example of a near surface environmental geophysics application, where an early warning detection to dynamic failure is required. Passive monitoring has been shown to be sensitive to a continuous velocity change, prior to catastrophic slippage events (Mainsant et al., 2012). Provided these changes represent a perturbation of the local scattering properties it is expected that an active source coda based monitoring exper-

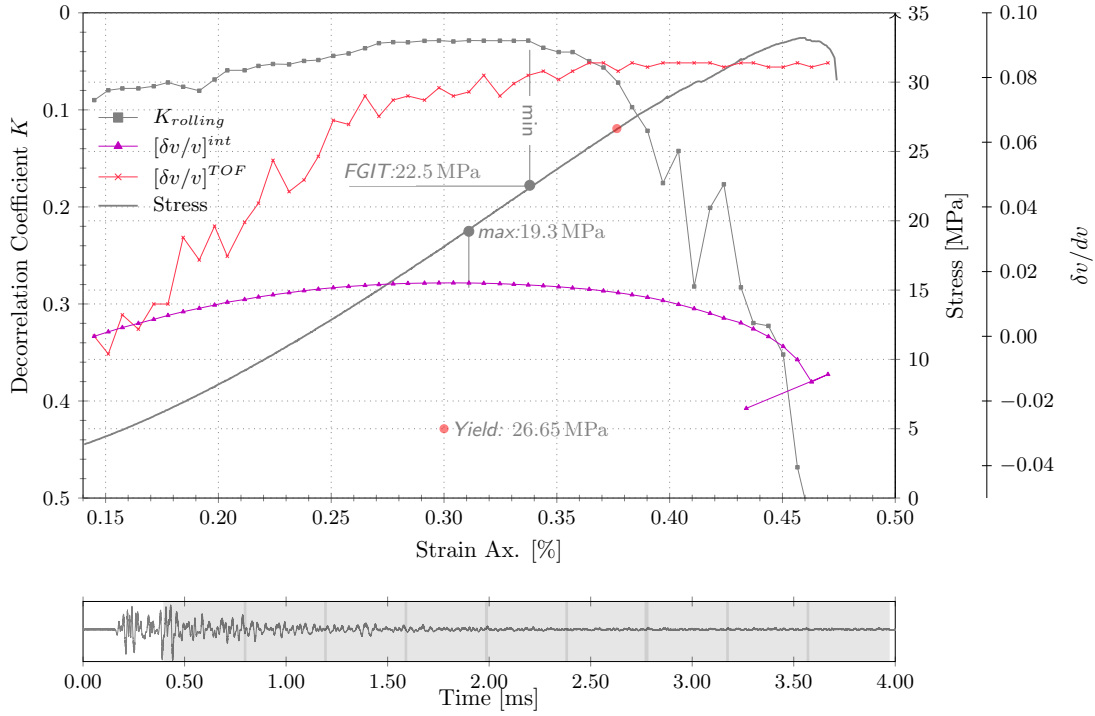


Fig. 4. (color online) CWD and CWI monitoring of BNT2. The $K_{rolling}$ and $[\delta v/v]^{int}$ trends are generated with a rolling lag equal to the repeat measurement frequency of 15 s (i.e. $N = 1$), calculated from 9 independent correlation windows .

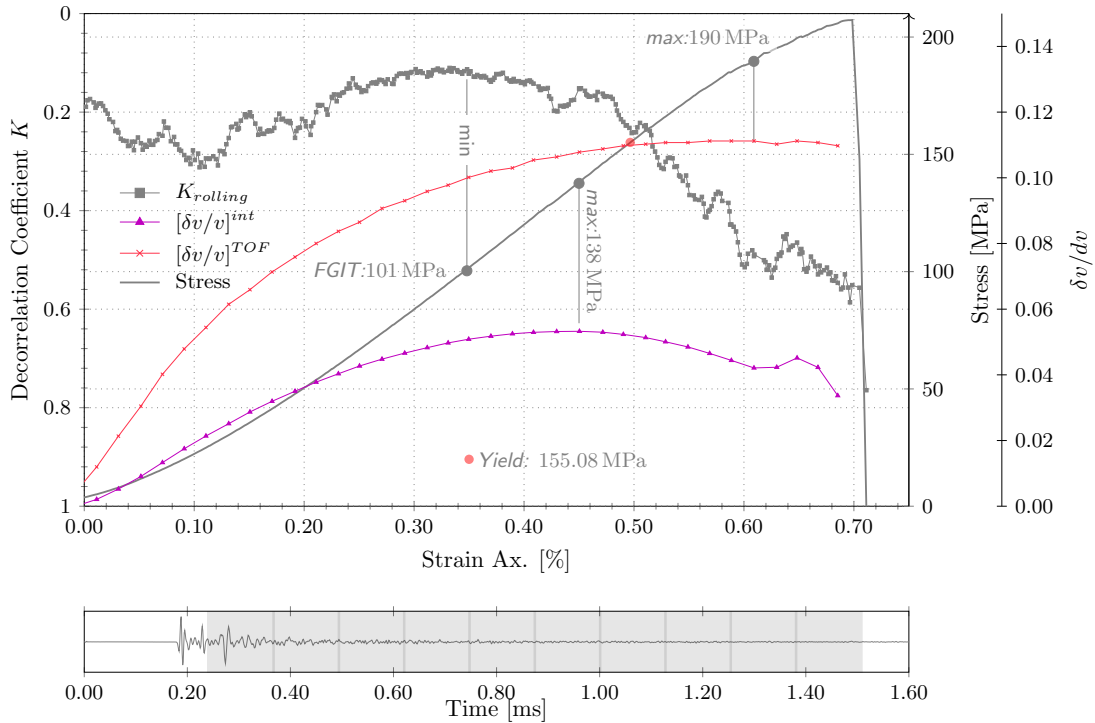


Fig. 5. (color online) Granite core (75.70 mm, ϕ 29.80 mm) from UCS test dataset for $N = (1, 10)$, $2t_w = 0.08$ msec and a 2.25 MHz source signature. Dataset: GRA.

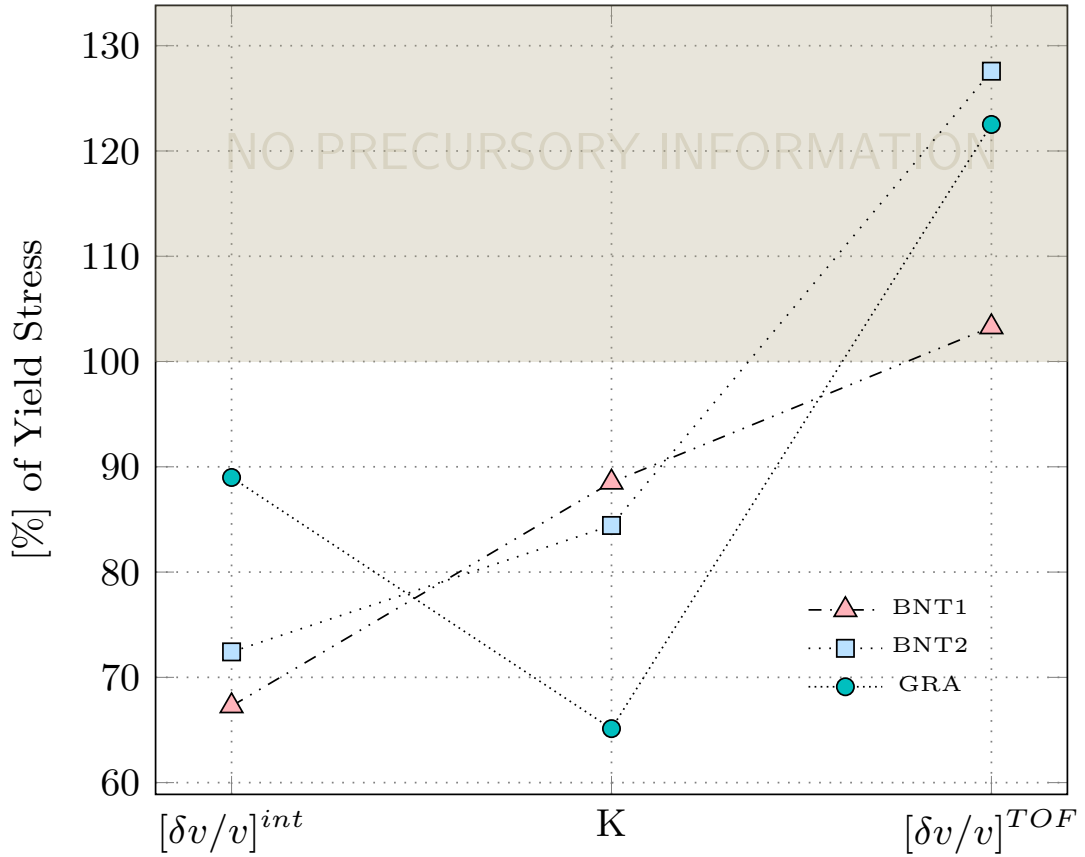


Fig. 6. (color online) Comparison of the precursory indicators to the Yield stress, determined from the rolling reference integrated relative velocity changes $[\delta v/v]^{int}$, the rolling reference decorrelation coefficient $K_{rolling}$, and the TOF derived relative velocity changes $[\delta v/v]^{TOF}$.

iment will provide similar sensitivity to precursory material yielding as shown for UCS tests.

Induced seismicity monitoring such as that associated with reservoir production (Bourne et al., 2014; van Thienen-Visser and Breunese, 2015) is typically driven by large field scale compaction as depletion of the pore-pressure occurs. Under such forces the reservoir will experience continuously evolving scattering properties, with both small undetectable and larger seismicity events. As with the San Andreas Fault Observatory at Depth - SAFOD (Zoback et al., 2011) fault damage zones monitoring, a continuous active source setup, will perhaps be able to identify inelastic changes which are undetectable with passive monitoring. Combining this with a rolling reference coda analysis will likely provide for a robust continuous reservoir monitoring setup where induced seismicity is of concern.

In the context of this study, the ability to determine the subtle onset of material yielding is possible with only the knowledge that loading occurs at a constant strain rate, and in the absence of direct stress and strain measurements. Provided an appropriate source frequency is practical, it is expected that this approach could be successfully applied to a wide variety of applications, such as the above mentioned structural-health, landslide, and compaction related induced seismicity monitoring. While these applications require additional investigation they can all be generalised as monitoring scenarios where

both high rate-of-change and long-term transient changes in material scattering properties are of concern. It is therefore expected that with an approximate knowledge of the underlying direction and type of perturbation, rolling reference coda based can monitoring can be applied to a wide variety of scales.

ACKNOWLEDGMENTS

We would like to thank Dayan Draganov, Cornelis Weemstra, Kees Wapenaar, Christian Reinicke, Lisanne Douma and Richard Bakker for their fruitful discussion throughout this work. A special thanks goes to the laboratory support staff at TUDelft, and specifically Karel Heller for his assistance in setting up an automated ultrasonic acquisition system for our experimental work. The recorded data used in this study can be found on <https://data.4tu.nl> under DOI uuid:e3071a50-7310-4609-95a1-6f8e69e556e2.

APPENDIX

The yield point of a stress(σ)-strain(ϵ) curve is determined by a search for the most linear region. This is achieved by fitting q lines to the trend as described by,

$$\sigma_i^{fit} = \beta_0 + \beta_1 \epsilon_i \Big|_{i=1}^m, \quad (15)$$

and assessing the most linear on the conditions that the slope β_1 is at a maximum and the fitting error at the end of the line is less than 2%.

$$\beta_{q,1} > \beta_{q-1,1} \quad (16)$$

$$\Delta(\sigma_{q,m}^{fit}, \sigma_{q,m}) < 2\% \quad (17)$$

Here m is selected to be approximately half the length of the linear elastic region in terms of sample points. The yield point is then defined at the end of the fitted line with maximum slope β_1 and fitting error $< 2\%$.

REFERENCES

- Aki, K. and Chouet, B. (1975). Origin of coda waves: Source, attenuation, and scattering effects. *Journal of Geophysical Research*, 80(23):3322.
- Barnhoorn, A., Cox, S. F., Robinson, D. J., and Senden, T. (2010). Stress- and fluid-driven failure during fracture array growth: Implications for coupled deformation and fluid flow in the crust. *Geology*, 38(9):779–782.
- Bieniawski, Z. T. (1967). Mechanism of brittle fracture of rock; Part I-theory of the fracture process. *International Journal of Rock Mechanics and Mining Sciences*, 4:395–406.
- Bourne, S. J., Oates, S. J., van Elk, J., and Doornhof, D. (2014). A seismological model for earthquakes induced by fluid extraction from a subsurface reservoir. *Journal of Geophysical Research: Solid Earth*, 119(12):8991–9015.
- Brownjohn, J. M. W. (2007). Structural health monitoring of civil infrastructure. *Philosophical Transactions of the Royal Society A: Mathematical, Physical and Engineering Sciences*, 365(1851):589–622.
- Ebisuzaki, W. (1997). A method to estimate the statistical significance of a correlation when the data are serially correlated. *Journal of Climate*, 10(9):2147–2153.
- Elliott, G. M. and Brown, E. T. (1986). Further development of a plasticity approach to yield in porous rock. *International Journal of Rock Mechanics and Mining Sciences and*, 23(2):151–156.
- Grêt, A. (2005). Monitoring rapid temporal change in a volcano with coda wave interferometry. *Geophysical Research Letters*, 32(6):L06304.
- Grêt, A., Snieder, R., and Scales, J. (2006). Time-lapse monitoring of rock properties with coda wave interferometry. *Journal of Geophysical Research: Solid Earth*, 111(3):1–11.
- Heap, M. and Faulkner, D. (2008). Quantifying the evolution of static elastic properties as crystalline rock approaches failure. *International Journal of Rock Mechanics and Mining Sciences*, 45(4):564–573.
- Larose, E., Planes, T., Rossetto, V., and Margerin, L. (2010). Locating a small change in a multiple scattering environment. *Applied Physics Letters*, 96(20).
- Li, C., Prikryl, R., and Nordlund, E. (1998). The stress-strain behaviour of rock material related to fracture under compression. *Engineering Geology*, 49(3-4):293–302.
- Mainsant, G., Larose, E., Brönnimann, C., Jongmans, D., Michoud, C., and Jaboyedoff, M. (2012). Ambient seismic noise monitoring of a clay landslide: Toward failure prediction. *Journal of Geophysical Research: Earth Surface*, 117(F1):n/a–n/a.
- Matsumoto, S., Obara, K., Yoshimoto, K., Saito, T., Ito, A., and Hasegawa, A. (2001). Temporal change in P-wave scatterer distribution associated with the M 6.1 earthquake near Iwate volcano, northeastern Japan. *Geophysical Journal International*, 145(1):48–58.
- Mogi, K. (2007). *Experimental rock mechanics*. CRC Press.
- Obermann, A., Planes, T., Larose, E., and Campillo, M. (2013). Imaging preeruptive and coeruptive structural and mechanical changes of a volcano with ambient seismic noise. *Journal of Geophysical Research: Solid Earth*, 118(12):6285–6294.
- Page, J. H., Cowan, M. L., and Weitz, D. A. (2000). Diffusing acoustic wave spectroscopy of fluidized suspensions. *Physica B: Condensed Matter*, 279(1-3):130–133.
- Paterson, M. S. and Wong, T. F. (2005). *Experimental Rock Deformation — The Brittle Field*. Springer-Verlag, Berlin/Heidelberg.
- Peksa, A. E., Wolf, K. H. A., and Zitha, P. L. (2015). Bentheimer sandstone revisited for experimental purposes. *Marine and Petroleum Geology*, 67:701–719.
- Pine, D., Weitz, D., Zhu, J., and Herbolzheimer, E. (1990). Diffusing-wave spectroscopy: dynamic light scattering in the multiple scattering limit. *Journal de Physique*, 51(18):2101–2127.
- Poupinet, G., Ellsworth, W. L., and Frechet, J. (1984). Monitoring velocity variations in the crust using earthquake doublets: An application to the Calaveras Fault, California. *Journal of Geophysical Research*, 89(B7):5719.
- Ratdomopurbo, A. and Poupinet, G. (1995). Monitoring a temporal change of seismic velocity in a volcano: Application to the 1992 eruption of Mt. Merapi (Indonesia). *Geophysical Research Letters*, 22(7):775.
- Rossetto, V., Margerin, L., Planes, T., and Larose, É. (2011). Locating a weak change using diffuse waves: Theoretical approach and inversion procedure. *Journal of Applied Physics*, 109(3).
- Sato, H., Fehler, M. C., and Maeda, T. (2012). *Seismic Wave Propagation and Scattering in the Heterogeneous Earth : Second Edition*, volume 9783642230. Springer Berlin Heidelberg, Berlin, Heidelberg.
- Sens-Schönfelder, C. and Larose, E. (2008). Temporal changes in the lunar soil from correlation of diffuse vibrations. *Physical Review E - Statistical, Nonlinear, and Soft Matter Physics*, 78(4):1–4.
- Sens-Schönfelder, C. and Wegler, U. (2006). Passive image interferometry and seasonal variations of seismic velocities at Merapi Volcano, Indonesia. *Geophysical Research Letters*, 33(21):L21302.
- Snieder, R. (2006). The Theory of Coda Wave Interferometry. *Pure and Applied Geophysics*, 163(2-3):455–473.
- Snieder, R., Douma, H., and Scales, J. (2002). Coda Wave Interferometry for Estimating Nonlinear Behavior in Seismic Velocity. *Science*, 295(March):2253–2255.
- Staeli, M., Saettele, M., Huggel, C., McArdell, B. W., Lehmann, P., Van Herwijnen, A., Berne, A., Schleiss, M.,

- Ferrari, A., Kos, A., Or, D., and Springman, S. M. (2015). Monitoring and prediction in early warning systems for rapid mass movements. *Natural Hazards and Earth System Sciences*, 15(4):905–917.
- Stähler, S. C., Sens-Schönfelder, C., and Niederleithinger, E. (2011). Monitoring stress changes in a concrete bridge with coda wave interferometry. *The Journal of the Acoustical Society of America*, 129(4):1945–1952.
- van Thienen-Visser, K. and Breunese, J. N. (2015). Induced seismicity of the Groningen gas field: History and recent developments. *The Leading Edge*, 34(6):664–671.
- Zhang, Y., Abraham, O., Grondin, F., Loukili, A., Tournat, V., Duff, A. L., Lascoup, B., and Durand, O. (2012). Study of stress-induced velocity variation in concrete under direct tensile force and monitoring of the damage level by using thermally-compensated Coda Wave Interferometry. *Ultrasonics*, 52(8):1038–1045.
- Zhang, Y., Planes, T., Larose, E., Obermann, A., Rospars, C., and Moreau, G. (2016). Diffuse ultrasound monitoring of stress and damage development on a 15-ton concrete beam. *The Journal of the Acoustical Society of America*, 139(4):1691–1701.
- Zoback, M., Hickman, S., and Ellsworth, W. (2011). Scientific Drilling Into the San Andreas Fault Zone—An Overview of SAFOD’s First Five Years. *Scientific Drilling*, (11, March 2011):14–28.